

PDF hosted at the Radboud Repository of the Radboud University Nijmegen

The following full text is a preprint version which may differ from the publisher's version.

For additional information about this publication click this link.

<http://hdl.handle.net/2066/103927>

Please be advised that this information was generated on 2019-02-19 and may be subject to change.

CHANDRA-HETGS OBSERVATIONS OF THE BRIGHTEST FLARE SEEN FROM Sgr A*

M. A. NOWAK¹, J. NEILSEN¹, S. B. MARKOFF², F. K. BAGANOFF¹, D. PORQUET³, N. GROSSO³, Y. LEVIN^{4,5}, J. HOUCK¹, A. ECKART⁶, H. FALCKE^{7,8,9}, L. JI¹⁰, J. M. MILLER¹¹, Q. D. WANG¹²

Submitted 2012 June 14. Resubmitted 2012 September 4. Accepted ...

ABSTRACT

Starting in 2012, we began an unprecedented observational program focused on the supermassive black hole in the center of our Galaxy, Sgr A*, utilizing the High Energy Transmission Gratings Spectrometer (HETGS) instrument on the *Chandra X-ray Observatory*. These observations will allow us to measure the quiescent X-ray spectra of Sgr A* for the first time at both high spatial and spectral resolution. The X-ray emission of Sgr A*, however, is known to flare roughly daily by factors of a few to ten times over quiescent emission levels, with rarer flares extending to factors of greater than 100 times quiescence. Here we report an observation performed on 2012 February 9 wherein we detected what is the highest peak flux and fluence flare ever observed from Sgr A*. The flare, which lasted for 5.6 ks and had a decidedly asymmetric profile with a faster decline than rise, achieved a mean absorbed 2–8 keV flux of $(8.5 \pm 0.9) \times 10^{-12} \text{ erg cm}^{-2} \text{ s}^{-1}$. The peak flux was 2.5 times higher, and the total 2–10 keV emission of the event was approximately 10^{39} erg. Only one other flare of comparable magnitude, but shorter duration, has been observed in Sgr A* by *XMM-Newton* in 2002 October. We perform spectral fits of this *Chandra* observed flare, and compare our results to the two brightest flares ever observed with *XMM-Newton*. We find good agreement among the fitted spectral slopes ($\Gamma \sim 2$) and X-ray absorbing columns ($N_{\text{H}} \sim 15 \times 10^{22} \text{ cm}^{-2}$) for all three of these events, resolving prior differences (which are most likely due to the combined effects of pileup and spectral modeling) among *Chandra* and *XMM-Newton* observations of Sgr A* flares. We also discuss fits to the quiescent spectra of Sgr A*.

Subject headings: accretion, accretion disks – black hole physics – radiation mechanisms:nonthermal

1. INTRODUCTION

Sagittarius (Sgr) A* is the compact radio, infrared and X-ray source associated with the $4 \times 10^6 M_{\odot}$ supermassive black hole at the dynamical center of our Galaxy (see, e.g., Melia & Falcke 2001; Genzel et al. 2010). As the nearest galactic nucleus, Sgr A* offers unique access to accretion physics on event horizon scales, and is thus a key testbed for theoretical modeling. On the other hand in the almost 40 years since its radio identification (Balick & Brown 1974), a multitude of observational campaigns in the radio/millimeter, near-infrared (NIR) and X-ray bands have established that Sgr A* is emitting steadily at a bolometric lu-

minosity $L_{\text{Bol}} \sim 10^{-9} L_{\text{Edd}}$, orders of magnitude lower than is typical for nearby low-luminosity active galactic nuclei (LLAGN; e.g., Ho 1999). Sgr A* is thus either representative of a distinct class of quiescent galactic nuclei lurking within most normal galaxies, or it is simply occupying the extreme low end of the AGN continuum (see, e.g., Nagar et al. 2005, Figure 4). Placing Sgr A* into context with other objects is therefore an important goal, in order to correctly interpret its rather atypical features.

The X-ray band is a powerful probe of the inner accretion flow regions of black holes. The *Chandra X-ray Observatory* soon after its launch was the first to identify Sgr A* by discovering a dominant, steady emission state (Baganoff et al. 2003) which can just be spatially resolved at *Chandra*'s sub-arcsecond imaging resolution. This emission can be associated with thermal bremsstrahlung from near the gravitational capture radius (Quataert 2002; but see Sazonov et al. 2012 for an alternative). The X-ray “quiescent state” is punctuated roughly daily by flares with \lesssim hour time scales that point to a source within $\sim 10^3$ s of $r_g \equiv GM/c^2$ (the gravitational radius) from the black hole (Baganoff et al. 2001; Goldwurm et al. 2003; Bélanger et al. 2005; Porquet et al. 2003, 2008). The flares, whose emission has been modeled with synchrotron or alternatively inverse Compton, are most likely caused by nonthermal processes (e.g., shock or magnetic reconnection acceleration of electrons within a jet; Markoff et al. 2001; Yuan et al. 2004; Yusef-Zadeh et al. 2006; Dodds-Eden et al. 2009), though other mechanisms have also been suggested (e.g., Liu & Melia 2002; Zubovas et al. 2012).

Simultaneous monitoring campaigns with the NIR have established that all the X-ray flares have NIR counterparts, while only the brighter NIR flares (≥ 10 mJy) have corresponding X-ray activity (Eckart et al. 2004; Ghez et al. 2004; Hornstein et al. 2007; Dodds-Eden et al. 2009, 2011;

¹ Massachusetts Institute of Technology, Kavli Institute for Astrophysics, Cambridge, MA 02139, USA; mnnowak,jneilsen,fbk,houck@space.mit.edu

² Astronomical Institute, “Anton Pannekoek”, University of Amsterdam, Amsterdam, The Netherlands; s.b.markoff@uva.nl

³ Observatoire Astronomique de Strasbourg, Université de Strasbourg, CNRS, UMR 7550, 11 rue de l’Université, 67000 Strasbourg, France; delphine.porquet,nicolas.grosso@astro.unistra.fr

⁴ School of Physics and CSPA, Monash University, VIC 3800, Australia; Yuri.Levin@monash.edu

⁵ Leiden Observatory, Leiden University, P.O. Box 9513, NL-2300 RA Leiden, The Netherlands

⁶ Physikalisches Institut, Universität zu Köln, Zùlpicher Str. 77, 50937 Köln, Germany; eckart@ph1.uni-koeln.de

⁷ Department of Astrophysics, IMAPP, Radboud University Nijmegen, PO Box 9010, 6500 GL Nijmegen, The Netherlands; H.Falcke@astro.ru.nl

⁸ ASTRON, Postbus 2, 7990 AA Dwingeloo, the Netherlands

⁹ Max-Planck-Institut für Radioastronomie, Auf dem Hügel 69, 53121 Bonn, Germany

¹⁰ Purple Mountain Observatory, CAS, Nanjing, P.R. China, 210008; ji@pmo.ac.cn

¹¹ Department of Astronomy, University of Michigan, Ann Arbor, Michigan, MI 48109, USA; jonmm@umich.edu

¹² Department of Astronomy, University of Massachusetts, Amherst, MA 01002, USA; wqd@astro.umass.edu

Trap et al. 2011). The relationship of X-ray and NIR flaring to that in the sub-millimeter (submm) bands is still under debate, although broad peaks delayed from the NIR have been noted (Marrone et al. 2008; Yusef-Zadeh et al. 2006, 2008).

Many important questions persist about the nature of the accretion flow in Sgr A*, and particularly about the flares, which seem to provide a missing link with activity seen in other weakly accreting black holes. Specifically, in the last decade the Fundamental Plane (FP) of black hole accretion (Merloni et al. 2003; Falcke et al. 2004; K rding et al. 2006) has emerged as an important concept that links black hole mass and radiative output in the radio and X-ray bands for weakly accreting systems, with Sgr A* being an extreme low-luminosity example of such systems. As statistics have improved, it now appears that the X-ray flux of Sgr A* approaches or meets the expectations from the FP only during its flaring state, but lies at too low an X-ray flux, relative to its radio emission, during quiescence (Markoff 2005; K rding et al. 2006; Plotkin et al. 2012). As the FP radio luminosity is associated with synchrotron emission from accelerated particles in compact jets, the flares may be providing clues about jet launching and plasma processes near the black hole.

Only about two dozen X-ray flares have been detected so far, primarily with *Chandra* and *XMM-Newton*. Most flare fluxes are on the order of a factor of a few to ten times the quiescent flux, but a few show fluxes on the order of 100 times greater than quiescence, and sometimes have associated pre- or post-cursor ‘‘hiccups’’, i.e., weak flares close in time to the major outburst (Baganoff et al. 2001; Porquet et al. 2003, 2008). Exact flare characteristics such as spectral slope, which is very important for constraining models, are not well-determined because *Chandra* flares suffer pileup. Pileup in the Advanced CCD Imaging Spectrometer-Imaging array (ACIS-I; Garmire et al. 2003) is when two or more events arrive in overlapping pixel regions within the same detector readout frame, and subsequently are either read as a single event with the summed energy or are discarded as a non-X-ray event (Davis 2001). Although *XMM-Newton* flare observations do not suffer from pileup, its larger mirror point spread function (PSF) does not isolate the accretion flow as effectively. Prior studies had shown spectral slope differences between flares observed with *Chandra* and *XMM-Newton* (Baganoff et al. 2001; Porquet et al. 2003, 2008), and it has been unclear to what extent these differences were due to instrumental effects.

As part of an unprecedented X-ray Visionary Project (XVP) awarded in its Cycle 13 Guest Observer Program, *Chandra* has begun the first of a total of 3 Msec of observations to be carried out in 2012 with the High Energy Transmission Grating Spectrometer (HETGS; Canizares et al. 2005). The main goal of this program is to constrain the accretion processes around Sgr A*, including detecting flares for the first time with high-resolution spectroscopy ($E/\Delta E \approx 200@6.4\text{ keV}$). In our first several observations, already two major flaring periods have occurred, the first of which contains the brightest flare detected to date. This flare is sufficiently strong and long to allow us to create an individual spectrum. Here we present a detailed analysis of this flare and compare its spectra and characteristics to the two brightest X-ray flares reported in the last decade of Sgr A* observations. In addition we discuss the quiescent state, as observed in the 0th order of the gratings, and suggest a standardized method for reporting flare peaks

and spectra to aid in characterizing the flare distribution for studies of the entire sample of events.

2. OBSERVATIONS

At the time of writing of this paper, 2012 April 1, there have been 39 *Chandra* observations of Sgr A* using its ACIS-I, totaling 1.2 Msec, and now 10 using the HETG in combination with the ACIS-Spectroscopy array (ACIS-S), totaling 320 ks. The HETG is comprised of two gratings sets: the medium energy gratings (MEG) and the high energy gratings (HEG), which disperse spectra into positive and negative spectral orders. We consider only the HEG and MEG $\pm 1^{\text{st}}$ orders, which between them cover the $\approx 0.5\text{--}9\text{ keV}$ energy band. Additionally, an on-axis undispersed image is created at CCD spectral resolution (the 0th order). Compared to observations without insertion of the HETG, the 0th order efficiency ranges from $\approx 30\%$ at 2 keV to $\approx 80\%$ at 8 keV, with an average of $\approx 40\%$ when weighted by Sgr A*’s quiescent count rate spectrum.

The focus of our present work is a very bright flare observed with the HETGS during a 59.25 ks observation that began at 06:17:03 UTC on 2012 February 9 (ObsID 14392). The overall reduction in 0th order efficiency means that Sgr A* flares like this one are subject to significantly less photon pileup than ACIS-I observations conducted absent the gratings. (ACIS-S spectra also have slightly higher spectral resolution than ACIS-I spectra with comparable S/N.) The dispersed gratings spectra of Sgr A* flares are never subject to pileup. We leave the challenging analysis of the quiescent gratings spectra, which include significant background from diffuse Galactic center emission dispersed across the field of view, for a later date, when more data are available and we have a more reliable model of the background emission.

We took two steps to isolate Sgr A*’s flare emission and minimize the contribution from diffuse X-ray background. First, we extracted spectra and lightcurves from small circular regions with radii of 2.5 pixels ($\approx 1''/25$) centered on Sgr A*’s celestial coordinates¹. For the major flare discussed in this paper, we also extracted lightcurves and spectra for the $\pm 1^{\text{st}}$ order gratings (as determined by the `tg_resolve_events` tool) from long, 5 pixel wide rectangular regions centered on the dispersed spectra. Second, we reprocessed and extracted CCD spectra from all existing *Chandra* Sgr A* observations, including ACIS-I data, to provide the best possible characterization of the quiescent spectrum. All data were processed with standard CIAO v4.4 tools (Fruscione et al. 2006) and calibration database v4.4.8. We selected standard event grades (0, 2–4, 6) and applied corrections for Charge Transfer Inefficiency (CTI), but did not apply pixel randomization to the event positions. For ACIS-I and HETGS 0th order spectra, detector response matrices and effective areas were created with the `mkacisrmf` and `mkarf` tools², with the effective areas being ‘‘aperture corrected’’ using the `arfcorr` tool. (This tool divides the effective area by an energy-dependent fraction that ranged from $\approx 0.9\text{--}0.83$ between 2–8 keV, which accounts for the fraction of the energy-dependent, point source PSF within the 2.5 pixel radius source region.) Gratings responses were created with the `mkgrmf` (which includes flux aperture correction) and `mkgarf` tools (see Huenemoerder et al. 2011, for an outline of the gratings

¹ We did not re-register coordinates, since the latest *Chandra* data processing versions register Sgr A* to a positional accuracy of typically 0''/1.

² ACIS-I response matrices for ObsID 292, however, were created with the `mkxrmf` tool as this observation occurred at a -110 C focal plane temperature.

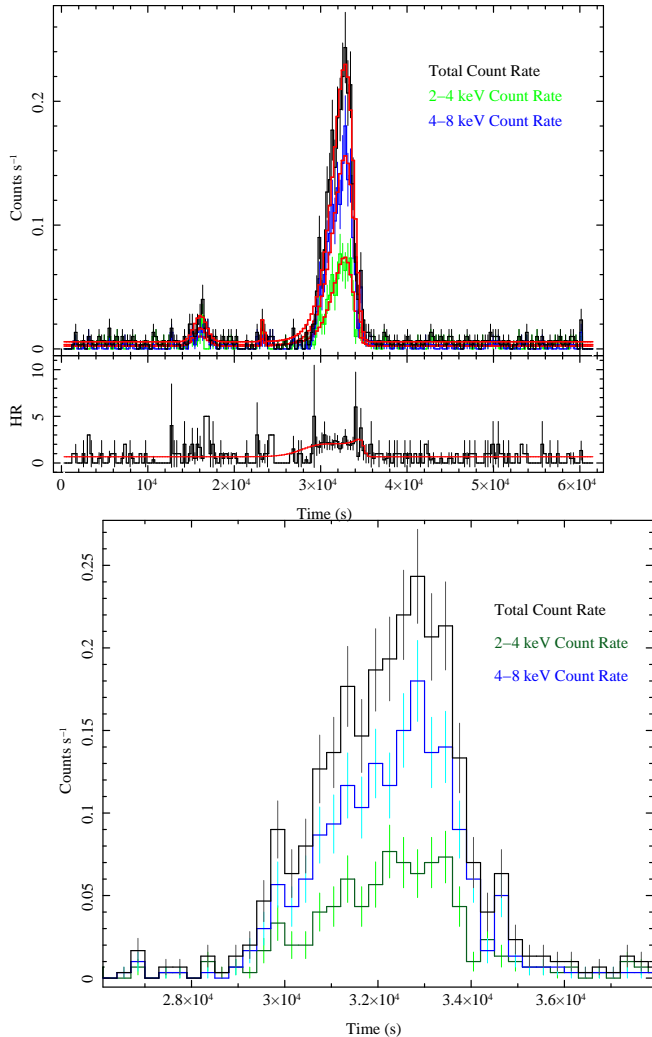


FIG. 1.— Top: 2–8 keV, 2–4 keV, and 4–8 keV Sgr A* lightcurves in 300 s bins from *Chandra* ObsID 14392, comprised of 0th order and $\pm 1^{\text{st}}$ order counts. Time is measured relative to the observation start: 2012 Feb. 9, 06:17:04 UTC. Each lightcurve is fit with a constant, two Gaussian distributions (for the precursor flares), and a Gumbel distribution. Middle: Hardness ratio of the 4–8 keV/2–4 keV rates, shown with the hardness ratio from the fits. Bottom: Close-up of the bright flare, highlighting its asymmetric profile.

processing procedures).

3. LIGHTCURVES

We searched for flares in the Sgr A* lightcurves by applying a Bayesian Blocks algorithm (Scargle 2002, priv. comm.) to unbinned events in the 2–9 keV band, using the implementation from the *S-lang/ISIS* Timing Analysis Routines³ (SITAR). This same method was employed previously by Baganoff et al. (2003). We chose a detection significance level of 98.2%, i.e., $1 - \exp(-4)$, for each lightcurve “change point”. Since a flare has at least two change points, a rise and a decay, the overall flare significance is at least 99.97%. Each lightcurve is then described by a series of uniform rate bins (usually only one bin for the mean rate). For lightcurves described by multiple bins, any bin with a rate below the $2\text{-}\sigma$ upper bound of the lowest rate bin was consid-

ered as “quiescent”, while the remaining bins were assigned as “flare”. Contiguous flare bins were considered to be a single flare, and were excised to create quiescent spectra for all observations. Using the Bayesian Blocks algorithm, we found 18 flares in the ACIS-I observations and 6 flares in the HETGS observations, with 2 in ObsID 14392. In a future work we will describe the statistics and properties of the full set of flares detected in all *Chandra* observations; however, here we are concerned with the second flare from ObsID 14392. Both the mean and peak count rates from this flare were significantly higher than any other observed *Chandra* flare.

Figure 1 presents the full, energy-resolved X-ray lightcurve for ObsID 14392, comprised of 0th and $\pm 1^{\text{st}}$ order events in 300 s bins. A large flare occurs roughly halfway through the observation and lasts ≈ 5 ks, with two possible precursor flares at $\sim 16,000$ s and $\sim 22,000$ s. The latter flare appears in the Bayesian Blocks lightcurve only if we decrease the detection significance level (for detecting two change points) to 93%. As discussed in Section 4, we create spectra for the mean of the large flare, but do not have sufficient statistics to describe the spectra at the flare peak. Determining the amplitude of the flare in the lightcurve is therefore particularly important for assessing the flare’s peak luminosity.

The precursor flares are rather faint; however, the main flare is clearly visible above the background level, which is composed of the quiescent emission from Sgr A* as well as diffuse emission throughout the extraction regions. The main flare is asymmetric (Figure 1, bottom), with a slow rise and a sharp decline, and can be modeled as a strong, wide ($\sigma \sim 1400$ s) Gaussian flare followed by a weaker, narrower ($\sigma \sim 400$ s) Gaussian flare approximately 1100 s later. However, since our primary focus is in determining the peak brightness of the flare, it is useful to have this quantity as a free parameter when fitting the lightcurve. We accomplish this with a renormalized Gumbel distribution:

$$f(t) = N_{\text{peak}} e^{(t-t_0)/\tau} e^{-\exp[(t-t_0)/\tau]}, \quad (1)$$

where N_{peak} is the peak count rate, t is time, t_0 is the peak time, and τ is the characteristic time scale. This provides a good match to the flare’s asymmetry (see the red curves in Figure 1). Our full model for the lightcurve consists of Gaussians for the two precursor flares and a Gumbel component for the main flare, superimposed on a constant baseline. The mean flare-only count rate, calculated over the interval where the main flare is brighter than the background level, is 0.091 ± 0.006 counts s⁻¹; the peak flare-only count rate is 0.22 ± 0.2 counts s⁻¹, and the characteristic time scale for the flare is 1180 ± 70 s. The error bars are 90% confidence intervals for a single parameter using the Cash statistic (Cash 1979). Thus the flare peak rate is 2.5 ± 0.3 times the mean flare count rate. This should be regarded as a lower limit, since the 0th order lightcurve is actually suppressed by pileup during the flare (see Figure 2 and the discussion below).

There is evidence for substructure in our Bayesian blocks decomposition of the flare (Figure 2): the peak of the flare is consistent with having a brief ≈ 300 s dip in between two sharp peaks of ≈ 100 s duration. This structure exists independently (albeit at lower significance) in both the 0th order and summed 1st order lightcurves. A similar dip/short time scale structure was seen in the 2002 October flare observed by *XMM-Newton* (Porquet et al. 2003).

We also have searched for any X-ray color differences between the flare and non-flare intervals. First, we calculated

³ <http://space.mit.edu/cxc/analysis/SITAR/>

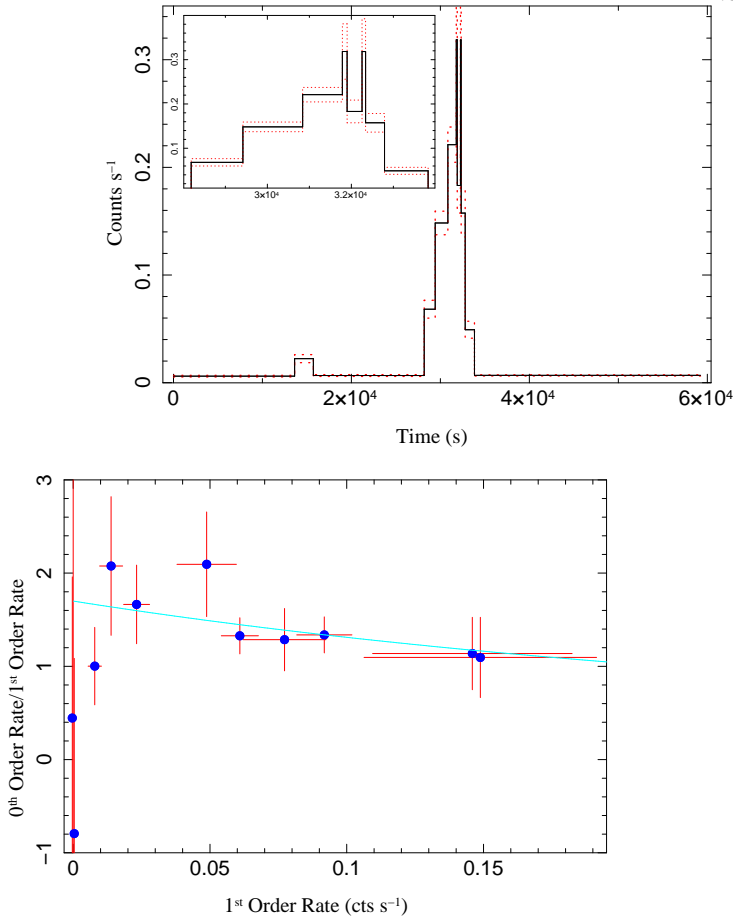


FIG. 2.— Top: For ObsID 14392, the summed 0th and 1st order count rates (solid line) with 1 σ errors (dotted line) during intervals found by the Bayesian Blocks algorithm (using a 98.2% significance level for each change point). The major flare start and stop times are 2012 Feb. 9, 14:25:50 and 15:59:51 UTC. Bottom: For each Bayesian Block, after subtracting the mean quiescent level rate, the ratio of the 0th order rate to the summed 1st order rates vs. the summed 1st order rates. (Error bars are 1 σ .) The light blue line is the expected correlation if the intrinsic (i.e., unpiled) 0th order rate is 1.7 \times the 1st order rate, and the pileup parameter $\alpha = 1$.

a hardness ratio (HR) as the ratio of the 4–8 keV lightcurve to the 2–4 keV lightcurve. Zeros in the denominator were replaced with the median 2–4 keV count rate. The results are shown in the bottom panel of Figure 1. The smooth red curve is the ratio of the fits to the relevant light curves, and the flare appears harder than the quiescent emission. A Kolmogorov-Smirnov (K-S) test on the extracted events indicates that the probability that the flare and quiescent intervals have the same spectrum is $P = 3 \times 10^{-15}$ (see Figure 3 for the cumulative distribution functions, i.e., CDFs). If we consider only events from the $\pm 1^{\text{st}}$ order gratings spectra or the 0th order, the probability that the flare and quiescent intervals have the same spectrum is $P = 3 \times 10^{-9}$ and $P = 4.6 \times 10^{-2}$, respectively. We conclude that at the $> 95\%$ level, the flare spectrum is harder than the quiescent spectrum. There is no evidence for a difference in the pre-flare and post-flare spectra, although the CDFs in Figure 3 do indicate that the ≈ 6.6 keV iron emission (Baganoff et al. 2003; Sazonov et al. 2012) is relatively significant in the quiescent spectrum, even in this short observation.

To search for evidence of any color evolution during the flare, we examine the ratio of the 0th order to summed 1st order count rates, as the former is most sensitive to hard X-

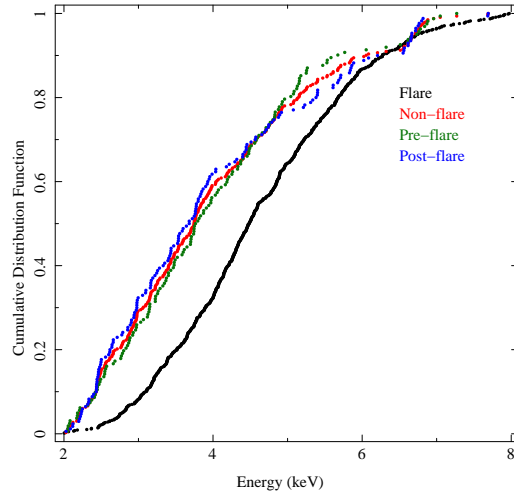


FIG. 3.— Cumulative distribution functions (CDFs) of the 0th and $\pm 1^{\text{st}}$ order counts as a function of energy for the main flare and the quiescent interval, further subdivided into pre- and post-main flare intervals. The quiescent and flare CDFs differ at $> 95\%$ confidence. The rise in the quiescent CDF at 6.6 keV indicates a strong contribution from the known iron emission.

rays while the latter is most sensitive to soft X-rays. Figure 2 shows this rate ratio for the lightcurve sub-intervals obtained from the Bayesian Blocks decomposition. Because the 0th order is still subject to pileup, this ratio can vary even in the absence of color evolution. For a constant spectral shape, the ratio of the 0th order counts and $\pm 1^{\text{st}}$ order counts should scale as:

$$(\alpha\Lambda_i)^{-1} [\exp(\alpha\Lambda_i) - 1] \exp(-\Lambda_i) , \quad (2)$$

where Λ_i is the incident (unpiled) counts per integration frame, and the odds of N piled photons being detected as a single “good event” is assumed to be $\propto \alpha^{(N-1)}$ (Davis 2001). The expected curve is shown in the bottom panel of Figure 2, under the assumption that all piled events are recorded (i.e., $\alpha = 1$) and that the gratings rate is $\approx 37\%$ of the total incident unpiled count rate. The data are consistent with no detectable spectral evolution during the flare, aside from pileup effects. We estimate that due to the effects of pileup, our lightcurve measurement of the peak/mean ratio is a factor ≈ 1.1 too low.

These naive estimates, however, are subject to systematic uncertainties in the details of the pileup model. For the 0th order spectra, we estimate that on average, 8% of the incident flare photons are subject to pileup, with this fraction increasing to 16% at the flare peak. Of the detected 0th order flare events, on average 0–4% (for $\alpha = 0$ –1) are in fact “piled” events falsely registered at higher energies that harden the spectrum. This systematic effect is accounted for in the 0th order spectral fits below, aided by the fact that the simultaneously fit HETGS spectra are not subject to pileup. Nevertheless, uncertainty in pileup modeling (specifically, α) serves to widen the error bars on the photon index fit to the flare spectra.

4. SPECTRA

We next consider the spectrum for the bright flare observed in ObsID 14392, and specifically compare it to Sgr A* quiescent spectra. It is not completely straightforward to characterize Sgr A*’s quiescent emission, as it is clearly extended (Shcherbakov & Baganoff 2010; Sazonov et al. 2012). In fact, recent models of the extended emission (i.e., Shcherbakov & Baganoff 2010) suggest that only on the order

TABLE 1
JOINT FIT TO CHANDRA FLARE AND QUIESCENT SPECTRA FROM THE SGR A* REGION

State	F_{2-8}^{abs} (10^{-12} erg cm^{-2} s^{-1})	F_{2-8}^{unabs} (10^{-12} erg cm^{-2} s^{-1})	F_{2-10}^{unabs} (10^{-12} erg cm^{-2} s^{-1})	L_{2-10}^{unabs} (10^{34} erg s^{-1})	F_{ν}^{abs} (nJy)	N_{H} (10^{22} cm^{-2})	Γ	E_{line}	σ_{line} (keV)	EW	χ^2/DoF
Flare Mean	$8.5^{+0.9}_{-0.9}$	$21.6^{+10.3}_{-5.2}$	$25.1^{+9.4}_{-4.8}$	$19.2^{+7.2}_{-3.7}$	770	$14.3^{+4.4}_{-3.6}$	$2.0^{+0.7}_{-0.6}$	267/256
Quiescent	$0.147^{+0.004}_{-0.003}$	$0.45^{+0.04}_{-0.04}$	$0.47^{+0.05}_{-0.03}$	$0.36^{+0.04}_{-0.04}$	9.6	$12.9^{+0.8}_{-0.8}$	$3.0^{+0.2}_{-0.2}$	$6.63^{+0.02}_{-0.02}$	$0.02^{+0.04}_{-0.02}$	$0.78^{+0.14}_{-0.12}$	267/256
Flare Peak	21^{+3}_{-3}	54^{+27}_{-15}	63^{+25}_{-14}	48^{+19}_{-11}

NOTE. — The model, `dustscat` × `TBnew` × (`powerlaw` + `gaussian`), is applied separately to the quiescent spectrum and the flare spectrum. No gaussian is included during the flare. We model the 0th order spectrum during the flare as the sum of the quiescent emission and flare emission; for the HETG flare spectrum, we subtract the quiescent emission and diffuse extended emission as background. In lieu of model normalizations, we measure the integrated 2–8 and 2–10 keV fluxes F with the `cflux` convolution model. We report both absorbed (superscript abs) and unabsorbed (superscript unabs) fluxes; the 2–10 keV luminosity L presumes isotropic emission at a distance of 8 kpc. F_{ν}^{abs} is the best fit model flux density at 6 keV (no errors given). N_{H} is the equivalent hydrogen column density, Γ is the power law index, and E_{line} , σ_{line} , and EW are the energy, 1σ width, and equivalent width of the Gaussian emission line. Errors are 90% confidence level for one interesting parameter. Peak flux values are derived assuming a peak/mean flux ratio of 2.5 ± 0.3 (90% CL), with errors combined in quadrature. Due to pileup, this ratio may in fact be $\approx 10\%$ too low (see text).

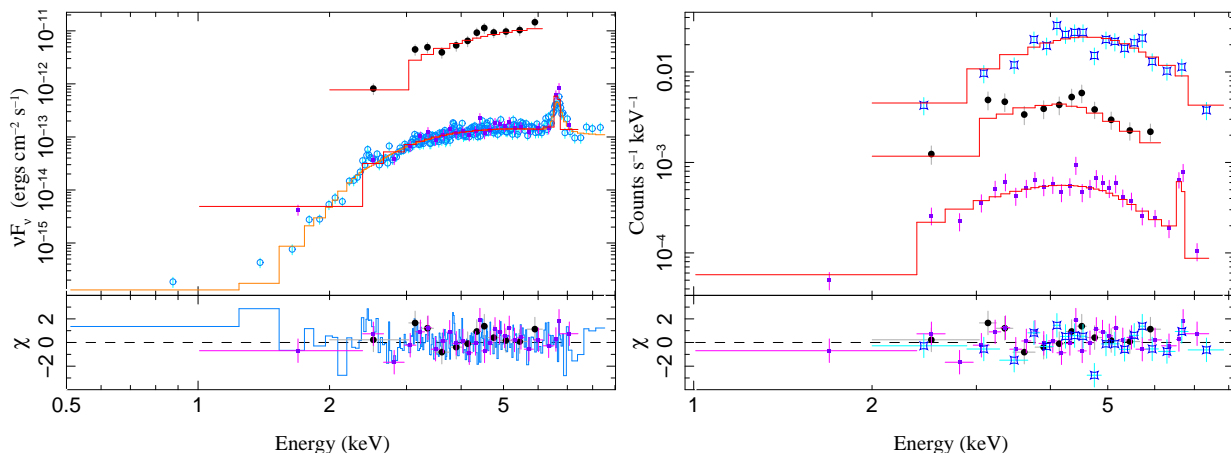


FIG. 4.— Left: Summed, flux corrected spectra for the inner $1''/25$ radius surrounding Sgr A*, with the fit presented in Table 1. Spectra represent: quiescent emission (ACIS-I, hollow blue circles; and HETG 0th order, solid purple squares), and the bright flare mean emission (HETG $\pm 1^{\text{st}}$ orders, solid black circles). Right: The same spectra (absent ACIS-I spectra) shown as detector counts $\text{s}^{-1} \text{keV}^{-1}$, and now including 0th order spectra for the flare (hollow blue squares).

of 1% of the observed quiescent emission arises near the event horizon, as opposed to flare models where, owing to time scales of only thousands of seconds, almost all the emission is associated with the inner region. We ignore these distinctions and do not break up the quiescent emission into “point-like” and “extended” components, nor do we even attempt to “background subtract” the quiescent emission. Instead, we use consistent extraction regions between the quiescent and flare periods, and treat the flare as *additional* emission. Since our quiescent spectra include diffuse emission, we generally prefer to report absolute flare flux levels, rather than describing the flare in terms of a “factor times quiescent emission.” The mean absorbed flux density in the 2–8 keV band is the quantity least subject to systematic uncertainty and most useful in comparing current and prior observations.

4.1. Methodology

To accomplish these measurements, we created a 0th order spectrum and $\pm 1^{\text{st}}$ order spectra for the 5600s interval of the brightest flare in ObsID 14392. In order to isolate the actual flare spectrum, it is important to have a reliable characterization of the quiescent spectrum. For the gratings, we created a background spectrum by extracting a 1st order spectrum from the quiescent periods of ObsID 14392. Because the 0th order spectral analysis of the flare is complicated by the presence of

pileup, we modeled the 0th order flare spectrum as the sum of a flare component and a quiescent component. To constrain the quiescent component, we created quiescent spectra from *all Chandra* observations of Sgr A*. We kept the ACIS-I and 0th order ACIS-S spectra separate, but fit them with a single model⁴. This method appears justified because our K-S test does not indicate a difference between the pre- and post-flare quiescent spectra, and because prior studies have suggested a fairly stable quiescent level (Shcherbakov & Baganoff 2010).

We restricted our fits of the quiescent ACIS-I spectra to the 0.5–9 keV band, the 0th order quiescent spectra to the 1–9 keV band, and the gratings spectra to the 2–9 keV band. All combined spectra were rebinned to have a minimum signal-to-noise of 4.5 in each energy bin, and the gratings spectra were further required to have a minimum of 16 pre-binning channels per final energy bin. Only those bins completely inside the above energy ranges were included in our analysis.

For clarity, we set out the details of our fitting process.

⁴ All analyses described in this paper have been performed with the Interactive Spectral Interpretation System (ISIS; Houck & Denicola 2000). Spectra for each ObsID and gratings arm were kept separate, but like groups were combined during analysis using the `combine_datasets` function. Plots also show the combined data, and when showing “flux corrected” data this correction has been implemented using only the detector response matrices, and not the fitted models.

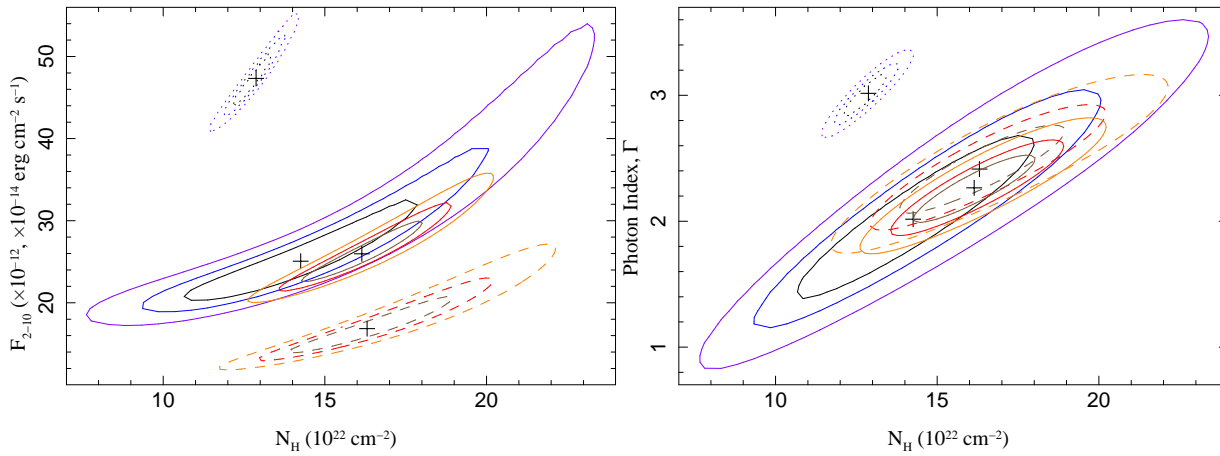


FIG. 5.— Confidence contours for Sgr A* spectral parameters at several epochs: mean unabsorbed 2–10 keV flux vs. X-ray absorbing column, N_{H} , (left) and photon index vs. N_{H} (right). Black/blue/purple lines are for the quiescent (dotted lines) and major flare (solid lines) emission observed by *Chandra* in ObsID 14392. Brown/red/orange lines are for flare emission observed by *XMM-Newton* on 2007 April 4 (dashed lines) and on 2002 October 3 (solid lines) (Porquet et al. 2003, 2008), re-analyzed with the same spectral model as applied to the *Chandra* observation. Contours are 68%, 90%, and 99% significance for two interesting parameters. Flare flux is in units of $10^{-12} \text{ erg cm}^{-2} \text{ s}^{-1}$ and quiescent flux is in units of $10^{-14} \text{ erg cm}^{-2} \text{ s}^{-1}$.

The quiescent spectra from ACIS-I and the 0th order were fit jointly with a single model consisting of an absorbed, dust-scattered power-law and an iron emission line (see below for details). The 1st order grating spectrum of the flare was modeled as a second absorbed, dust-scattered power-law, and the 0th order spectrum of the flare was treated as the sum of these two components convolved through the *ISIS* pileup model. (The pileup parameter α was left as a free parameter, but its error bars always spanned the full range 0–1. Again, this uncertainty contributes to widening the error bars on the fitted photon index, Γ .)

Although the overall spectral model is rather simple, the interstellar absorption and dust scattering components merit further discussion. X-ray absorption is dominated by metals, not hydrogen, hence the fitted hydrogen column is strongly dependent on the adopted cross sections and abundances (Wilms et al. 2000). We use the TBnew model⁵ developed from the work and abundances described by Wilms et al. (2000). In our experience, using TBnew with the cross sections of Verner et al. (1996) yields equivalent N_{H} values $\sim 1.5\times$ that of the oft used *wabs* model (Morrison & McCammon 1983).

For all intents and purposes, given the very small *Chandra* PSF, dust scattering acts as a pure loss term, with the dust scattering optical depth having an E^{-2} dependence. We use the model *dustscat* (see Baganoff et al. 2003), which has an optical depth at 1 keV proportional to the X-ray absorbing column density. This proportionality has been measured via dust scattering halo images and X-ray binary spectra obtained with *ROSAT* by Predehl & Schmitt (1995), who found $\tau \approx 0.486(N_{\text{H}}/10^{22} \text{ cm}^{-2})$ when using an analog of the *wabs* model and cross sections from Morrison & McCammon (1983). Given the rough scaling between TBnew and *wabs*, we tie our dust scattering optical depth to our fitted equivalent N_{H} via $\tau = 0.324(N_{\text{H}}/10^{22} \text{ cm}^{-2})$. The implied extinction (from the correlations of Predehl & Schmitt 1995) is then $A_{\text{V}} \sim N_{\text{H}}^{\text{TBnew}}/2.69 \times 10^{21} \text{ cm}^{-2}$. However, these dependencies have not been revisited with modern absorption or dust scattering models (e.g., Xiang et al. 2011, and references therein) using instruments capable of both imaging halos and making

direct measurement of metal absorption edges (i.e., *Chandra*-HETG and *XMM-Newton*-RGS), and must be treated as having a certain degree of systematic uncertainty. However, in regard to the values presented in Table 1, adopting a ratio of τ to $N_{\text{H}}/10^{22} \text{ cm}^{-2}$ that lies between 0.243–0.486 alters the implied X-ray fluxes by only $\pm 5\%$, our fitted N_{H} values by $\pm 10^{22} \text{ cm}^{-2}$, and our fitted photon indices by ± 0.05 .

4.2. Results

Our fit results are presented in Table 1 and are shown in Figure 4. Consistent with the results of the K-S test for the single ObsID 14392, the summed quiescent spectrum is significantly softer than the mean flare spectrum, with no overlap between the 90% confidence level error bars for their photon indices, Γ . The iron emission line at 6.63 keV in the quiescent spectrum has an equivalent width (EW) of $\approx 780 \text{ eV}$. If, instead of a power-law, we fit the quiescent continuum with a thermal plasma model that already includes ionized iron emission at a slightly higher energy than above (*vmekal*), we then find evidence for a 120 eV EW line at $6.3_{-0.1}^{+0.2} \text{ keV}$, consistent with Fe K α fluorescence, and consistent with the previous suggestion of such a line by Sazonov et al. (2012). This model provides a similarly good fit ($\chi^2/\text{DoF} = 264/256$) with plasma temperature $kT = 2.7_{-0.2}^{+0.3} \text{ keV}$ and a slightly smaller X-ray absorbing column density $N_{\text{H}} = (11.8_{-0.6}^{+0.7}) \times 10^{22} \text{ cm}^{-2}$. There is good agreement with previous studies of the quiescent spectrum (e.g., Baganoff et al. 2003; Sazonov et al. 2012), despite the fact that these authors used larger extraction regions ($1''$.5 radius) and very different background subtraction methods. We note that there is excellent agreement between the 0th order quiescent spectrum and the ACIS-I spectrum.

By any measure, the bright flare mean emission observed in ObsID 14392 is significantly brighter than the quiescent emission, and assuming that the peak spectrum has the same spectral shape as the mean spectrum, the peak emission is a factor of 2.5 times brighter still. The mean, absorbed 2–8 keV flux is higher than any Sgr A* mean flare flux observed with *Chandra*, and almost identical to the mean flux of the brightest Sgr A* flare ever observed by *XMM-Newton* (2002 October; Porquet et al. 2003, 2008, and Section 5). With a flare duration of $\approx 5.6 \text{ ks}$ (compared to $\approx 2.8 \text{ ks}$ for the

⁵ <http://pulsar.sternwarte.uni-erlangen.de/wilms/research/tbabs/index.html>

2002 October flare), the flare’s absorbed 2–8 keV fluence is $(4.7 \pm 0.5) \times 10^{-8} \text{ erg cm}^{-2}$, and its emitted intrinsic energy in the 2–10 keV band is approximately 10^{39} erg. As is evident in Table 1, the further we extrapolate beyond the well-measured 2–8 keV band, and if we consider unabsorbed instead of absorbed fluxes, the greater the uncertainty becomes both statistically and systematically.

Whereas the mean, absorbed flux is extremely well-constrained, the unabsorbed fluxes have strong dependencies upon the fitted X-ray absorbing column. Confidence contours for quiescent and mean unabsorbed flare flux vs. equivalent neutral column are presented in Figure 5. This figure also shows confidence contours for fitted photon indices, Γ , vs. equivalent neutral column. Unsurprisingly, there are strong correlations between indices and columns, with harder photon indices being associated with lower columns. There are, however, two important points to note: there is a good consistency between the fitted columns for the quiescent and flare spectra (with the latter allowing a wider range of values owing to the poorer statistics), and there is a very clear separation between the index/column contours for the quiescent and flare spectra. The flare spectrum is significantly harder; however, for most values of X-ray absorbing column the flare photon index is somewhat softer than implied by previous *Chandra* measurements of a bright flare that indicated $\Gamma = 1 \pm 0.8$ (90% confidence level; Baganoff et al. 2001). Absent the use of the HETGS, however, there is a question as to what extent this prior result was influenced by pileup. This prior result also used an earlier version of the *Chandra* calibration and did not include the E^{-2} dependence of dust scattering losses to the spectrum.

5. COMPARISON TO FLARES OBSERVED BY *XMM-Newton*

Our best-fit mean flare photon index of $\Gamma = 2_{-0.6}^{+0.7}$ is in good agreement with previous results obtained for the brightest (2002 October 3) and second brightest (2007 April 4) Sgr A* flares ever observed by *XMM-Newton* (Porquet et al. 2003, 2008), from 22 observations centered on Sgr A* which totaled 1.1 Msec through 2009 April. In order to carefully assess the degree to which the properties of the HETGS observed flare are comparable to the brightest *XMM-Newton* observed flares, we have re-fit the 2–10 keV spectra of the 2002 October 3 and 2007 April 4 flares — using the same data files as Porquet et al. (2008) — with the identical absorbed/scattered power-law model⁶ presented in Section 4.

For the 2002 October 3 flare we find a photon index $\Gamma = 2.3 \pm 0.3$, equivalent neutral column of $N_{\text{H}} = (16.1_{-2.2}^{+1.9}) \times 10^{22} \text{ cm}^{-2}$, and an unabsorbed 2–10 keV flux of $(26.0_{-3.5}^{+4.6}) \times 10^{-12} \text{ erg cm}^{-2} \text{ s}^{-1}$. This flare’s mean absorbed 2–8 keV flux is $(7.7 \pm 0.3) \times 10^{-12} \text{ erg cm}^{-2} \text{ s}^{-1}$, which for its 2.8 ks duration corresponds to an absorbed 2–8 keV fluence of $(2.2 \pm 0.1) \times 10^{-8} \text{ erg cm}^{-2}$ and an intrinsic emitted energy in the 2–10 keV band of 5.3×10^{38} erg. The photon indices found here are very similar to those reported in Porquet et al. (2008) with

a $\Delta\Gamma$ of only +0.1. The N_{H} values differ due to the different abundances and cross-sections assumed in this work.

We find a photon index of $\Gamma = 2.4_{-0.3}^{+0.4}$ for the 2007 April 4 flare, an equivalent neutral column of $N_{\text{H}} = (16.3_{-2.6}^{+3.0}) \times 10^{22} \text{ cm}^{-2}$, and an unabsorbed 2–10 keV flux of $(16.8_{-3.0}^{+4.6}) \times 10^{-12} \text{ erg cm}^{-2} \text{ s}^{-1}$. The mean absorbed 2–8 keV flux is $(4.8_{-0.3}^{+0.2}) \times 10^{-12} \text{ erg cm}^{-2} \text{ s}^{-1}$, which for the flare’s 2.9 ks duration corresponds to an absorbed 2–8 keV fluence of $(1.4 \pm 0.1) \times 10^{-8} \text{ erg cm}^{-2}$ and an intrinsic emitted energy in the 2–10 keV band of 3.5×10^{38} erg.

Figure 5 also presents confidence contours of X-ray absorbing column vs. 2–10 keV unabsorbed flux and photon index, Γ , for these two *XMM-Newton* observed flares. We see that the 2002 October and 2012 February events appear to be “twin flares” in all respects, and that aside from having a lower flux, the 2007 April flare otherwise appears identical to these two extremely bright flares. The *XMM-Newton* observed flares have slightly larger best-fit values for the equivalent neutral column; however, there is a high-degree of overlap among the error contours. Both *XMM-Newton* observed flares are also slightly shorter in duration, lasting ≈ 3 ks, with the brightest flare lightcurve also showing a brief dip near its peak, detected in all three EPIC instruments (Porquet et al. 2003, 2008).

6. DISCUSSION

Our *Chandra*-HETGS observation of Sgr A* taken on 2012 February 9 (ObsID 14392) exhibits a flare with the highest peak flux and fluence seen from this source. Remarkably, it is bright enough to allow the extraction of a pure flare gratings spectrum. Our comparative analysis indicates that in many ways, the bright Sgr A* flares observed by *XMM-Newton* in 2002 October and 2007 April are spectral twins to this flare. Depending upon how one defines and measures Sgr A*’s quiescent flux and in how one extrapolates the mean flare flux to a peak flux, for both the 2012 February and 2002 October flares, the ratio of peak flux to quiescent flux is at least a factor of order 130. If one adopts the suggestion of Shcherbakov & Baganoff (2010) that only $\approx 1\%$ of the observed quiescent flux is from the central regions (where the flare likely originates), then this factor is more plausibly of order 10^4 !

Given systematic uncertainties in extrapolating unabsorbed fluxes and defining the quiescent flux associated solely with the Sgr A* point source, however, we suggest that a less ambiguous set of reported values are the flare’s mean absorbed 2–8 keV flux, its absorbed 2–8 keV fluence, and the ratio of its peak rate to mean rate, each measured as values *above* the quiescent level and aperture corrected for the instrument’s PSF. So long as instrumental spectral extraction regions are consistent for quiescent and flare spectra, these values will be well-defined. (However, due to the short time scale sub-structure in the flare, as seen in Figure 2 and previously reported by Porquet et al. 2003, the “peak” flux value may actually be difficult to define precisely.) The 2–8 keV band is above the range of the most severe X-ray absorption in Sgr A* and is well-covered by the three soft X-ray instruments best capable of observing Sgr A*: *Chandra*, *XMM-Newton*, and *Swift*.

The bright flare is asymmetric, with a slower rise than decay. This may be due to unresolved sub-structure: the Bayesian Blocks decomposition shows evidence of complex structure near the flare peak, and a fit with two Gaussian profiles, with different widths and offset from one another, works well. (The fitted Gumbell profile is a convenience that allows

⁶ Porquet et al. (2003) analyzed the brightest *XMM-Newton* Sgr A* flare with a dust scattering model that presumed a fixed $A_{\text{V}} = 30$ (i.e., the scattering optical depth was not tied to the fitted N_{H}) and used the `tbabs` absorption model and abundances of Wilms et al. (2000) with the cross sections of Verner et al. (1996). Porquet et al. (2008), in order to compare to other works, instead analyzed the two brightest *XMM-Newton* flares with a dust scattering model with a fixed $A_{\text{V}} = 25$, and used `wabs` with cross sections of Morrison & McCammon (1983) and the abundances of Anders & Grevesse (1989).

us to easily calculate the flare peak/mean ratio.) Alternatively, if this is the flare’s intrinsic profile it is quite different than the “fast rise, exponential decay” of many different types of transient phenomena.

The total emitted 2–10 keV energy of the flare, which is of $\mathcal{O}(10^{39}$ erg), requires conversion of at least 10^{19} g of rest mass into energy, presuming a 10% conversion efficiency. There is no agreed upon mechanism for flare energization, with suggestions having ranged from magnetic reconnection (Markoff et al. 2001; Yuan et al. 2003; Dodds-Eden et al. 2010) to tidal disruption of asteroids (Čadež et al. 2008; Kostić et al. 2009; Zubovas et al. 2012). Regardless of the energization mechanism, with the results from the prior *XMM-Newton* observations it appears that at least these extremely bright flares require an emission mechanism that produces a moderate (i.e., not very hard) photon index, $\Gamma \approx 2$.

As we have shown, much of the uncertainty on the spectral slope is systematic, and depends on assumptions made about absorption and scattering. Reasonable assumptions about the scaling between dust scattering and absorption have only a small systematic effect ($\Delta\Gamma \sim 0.05$), but the dependence upon fitted N_{H} is more pronounced (i.e., Figure 5). Although there is a good consistency between the equivalent neutral column for the quiescent and flare spectra, it is possible to alter the fitted N_{H} by assuming different metal abundances, or metal depletions in dust grains, or different cross sections, etc. Based on the correlation from Predehl & Schmitt (1995) and our assumptions about N_{H} and A_{V} outlined in Section 4, the minimum reasonable X-ray absorbing column for the quiescent spectrum implies an extinction of $A_{\text{V}} \approx 40$. This is somewhat at odds with prior estimates of A_{V} : a discussion of the Galactic center optical and infrared extinction curves can be found in Fritz et al. (2011), who suggest a value of $A_{\text{V}} \approx 33$ (in part based upon the X-ray observations of Sgr A* discussed in Porquet et al. 2003). The relationships derived by Watson (2011) and Güver & Özel (2009), $A_{\text{V}} \approx N_{\text{H}}/2.2 \times 10^{21} \text{ cm}^{-2}$, imply a similar value for the extinction towards Sgr A*. However, the methods used to derive N_{H} and A_{V} in these works are very heterogeneous, and it is unclear if their scalings can be extrapolated to $A_{\text{V}} \sim 40$. It is therefore imperative that scaling between N_{H} , extinction, and dust scattering optical depth be revisited with modern models using consistent cross sections and abundances, and with modern high spectral and imaging resolution observations. For the moment, we conclude that the extinction, dust scattering optical depth, N_{H} , and (by extension) the spectral properties of Sgr A* are still subject to a certain degree of systematic uncertainty.

Despite these uncertainties, we find similar spectral properties for the brightest *Chandra* and *XMM-Newton* flares ($\Gamma \sim 2$

and $N_{\text{H}} \sim 15 \times 10^{22} \text{ cm}^{-2}$). Weaker flares could in principle have harder spectra than bright flares, but their spectral properties are not yet strongly constrained (as shown and discussed in Porquet et al. 2008). However, there is significant cause for optimism, as the observations discussed in this work represent slightly more than 10% of the *Chandra*-HETGS observations of Sgr A* that will occur in 2012. We anticipate that this program will detect over three dozen flares, with perhaps one or two more with amplitudes comparable to or greater than that of the 2012 February flare. As we have demonstrated that we can extract *Chandra* gratings spectra for *individual* bright flares, the XVP program should provide unprecedented constraints on the spectral properties of faint and moderate flares, which will allow us to determine how the physics of flares scales with their luminosity.

For the first time, the spatially resolved *Chandra* studies will produce Sgr A* flare spectra that are either absent of detector pileup or that have pileup strongly constrained (as is the case here) owing to the simultaneous 1st order gratings spectra. Our understanding of the physics of flares will be greatly enhanced by the fact that many of the upcoming observations will be performed with simultaneous multi-wavelength observations. The *Chandra* XVP program will offer us the unique opportunity to study the physics underlying accretion onto Sgr A* and other quiet galaxies.

We would like to thank all the members of the Sgr A* *Chandra*-XVP team⁷. We would also like to thank the *Chandra* schedulers for their continued superb support of this challenging program. We thank Jörn Wilms for useful discussions concerning absorption and extinction models. Michael Nowak, Joey Neilsen, and John Houck gratefully acknowledge funding support from the National Aeronautics and Space Administration through the Smithsonian Astrophysical Observatory contract SV3-73016 to MIT for support of the *Chandra* X-ray Center, which is operated by the Smithsonian Astrophysical Observatory for and on behalf of the National Aeronautics Space Administration under contract NAS8-03060. Fred Baganoff was supported by NASA Grant NAS8-00128. Fred Baganoff, Michael Nowak, and John Houck also were supported by NASA Grant GO2-13110A. Sera Markoff is grateful for support from a Netherlands Organization for Scientific Research (NWO) Vidi Fellowship, as well as from The European Community’s Seventh Framework Programme (FP7/2007-2013) under grant agreement number ITN 215212 “Black Hole Universe”. This work was based in part on observations obtained with *XMM-Newton*, an ESA science mission with instruments and contributions directly funded by ESA Member States and NASA.

REFERENCES

- Anders, E., & Grevesse, N. 1989, *Geochim. Cosmochim. Acta*, 53, 197
 Baganoff, F. K., Bautz, M. W., Brandt, W. N., et al. 2001, *Nature*, 413, 473
 Baganoff, F. K., Maeda, Y., Morris, M., et al. 2003, *ApJ*, 591, 891
 Balick, B., & Brown, R. L. 1974, *ApJ*, 194, 265
 Bélanger, G., Goldwurm, A., Melia, F., et al. 2005, *ApJ*, 635, 1095
 Canizares, C. R., Davis, J. E., Dewey, D., et al. 2005, *PASP*, 117, 1144
 Cash, W., 1979, *ApJ*, 228, 939
 Davis, J. E., 2001, *ApJ*, 562, 575
 Dodds-Eden, K., Gillessen, S., Fritz, T. K., et al. 2011, *ApJ*, 728, 37
 Dodds-Eden, K., Porquet, D., Trap, G., et al. 2009, *ApJ*, 698, 676
 Dodds-Eden, K., Sharma, P., Quataert, E., et al. 2010, *ApJ*, 725, 450
 Eckart, A., Baganoff, F. K., Morris, M., et al. 2004, *A&A*, 427, 1
 Falcke, H., Körding, E., & Markoff, S. 2004, *A&A*, 414, 895
 Fritz, T. K., Gillessen, S., Dodds-Eden, K., et al. 2011, *ApJ*, 737, 73
 Fruscione, A., McDowell, J. C., Allen, G. E., et al. 2006, in *Society of Photo-Optical Instrumentation Engineers (SPIE) Conference Series*, Vol. 6270, *Society of Photo-Optical Instrumentation Engineers (SPIE) Conference Series*
 Garmire, G. P., Bautz, M. W., Ford, P. G., Nousek, J. A., & Ricker, Jr., G. R. 2003, in *Society of Photo-Optical Instrumentation Engineers (SPIE) Conference Series*, ed. J. E. Truemper & H. D. Tananbaum, Vol. 4851, *Society of Photo-Optical Instrumentation Engineers (SPIE) Conference Series*, 28
 Genzel, R., Eisenhauer, F., & Gillessen, S. 2010, *Reviews of Modern Physics*, 82, 3121
 Ghez, A. M., Wright, S. A., Matthews, K., et al. 2004, *ApJ*, 601, L159

⁷ www.sgra-star.com/index.php/menu-collaboration-members

- Goldwurm, A., Brion, E., Goldoni, P., et al. 2003, *ApJ*, 584, 751
Güver, T., & Özel, F. 2009, *MNRAS*, 400, 2050
Ho, L. C., 1999, *ApJ*, 516, 672
Hornstein, S. D., Matthews, K., Ghez, A. M., et al. 2007, *ApJ*, 667, 900
Houck, J. C., & Denicola, L. A. 2000, in *ASP Conf. Ser. 216: Astronomical Data Analysis Software and Systems IX*, Vol. 9, 591
Huenemoerder, D. P., Mitschang, A., Dewey, D., et al. 2011, *AJ*, 141, 129
Körding, E., Falcke, H., & Corbel, S. 2006, *A&A*, 456, 439
Kostić, U., Čadež, A., Calvani, M., & Gomboc, A. 2009, *A&A*, 496, 307
Liu, S., & Melia, F. 2002, *ApJ*, 566, L77
Markoff, S., 2005, *ApJ*, 618, L103
Markoff, S., Falcke, H., Yuan, F., & Biermann, P. L. 2001, *A&A*, 379, L13
Marrone, D. P., Baganoff, F. K., Morris, M. R., et al. 2008, *ApJ*, 682, 373
Melia, F., & Falcke, H. 2001, *ARA&A*, 39, 309
Merloni, A., Heinz, S., & di Matteo, T. 2003, *MNRAS*, 345, 1057
Morrison, R., & McCammon, D. 1983, *ApJ*, 270, 119
Nagar, N. M., Falcke, H., & Wilson, A. S. 2005, *A&A*, 435, 521
Plotkin, R. M., Markoff, S., Kelly, B. C., Körding, E., & Anderson, S. F. 2012, *MNRAS*, 419, 267
Porquet, D., Grosso, N., Predehl, P., et al. 2008, *A&A*, 488, 549
Porquet, D., Predehl, P., Aschenbach, B., et al. 2003, *A&A*, 407, L17
Predehl, P., & Schmitt, J. H. M. M. 1995, *A&A*, 293, 889
Quataert, E., 2002, *ApJ*, 575, 855
Sazonov, S., Sunyaev, R., & Revnivtsev, M. 2012, *MNRAS*, 420, 388
Schlegel, D. J., Finkbeiner, D. P., & Davis, M. 1998, *ApJ*, 500, 525
Shcherbakov, R. V., & Baganoff, F. K. 2010, *ApJ*, 716, 504
Trap, G., Goldwurm, A., Dodds-Eden, K., et al. 2011, *A&A*, 528
Trap, G., Goldwurm, A., Terrier, R., et al. 2010, *Advances in Space Research*, 45, 507
Čadež, A., Calvani, M., & Kostić, U. 2008, *A&A*, 487, 527
Verner, D. A., Ferland, G. J., Korista, K. T., & Yakovlev, D. G. 1996, *ApJ*, 465, 487
Watson, D., 2011, *A&A*, 533, A16
Wilms, J., Allen, A., & McCray, R. 2000, *ApJ*, 542, 914
Xiang, J., Lee, J. C., Nowak, M. A., & Wilms, J. 2011, *ApJ*, 738, 75
Yuan, F., Quataert, E., & Narayan, R. 2003, *ApJ*, 598, 301
Yuan, F., Quataert, E., & Narayan, R. 2004, *ApJ*, 606, 894
Yusef-Zadeh, F., Bushouse, H., Dowell, C. D., et al. 2006, *ApJ*, 644, 198
Yusef-Zadeh, F., Wardle, M., Heinke, C., et al. 2008, *ApJ*, 682, 361
Zubovas, K., Nayakshin, S., & Markoff, S. 2012, *MNRAS*, 421, 1315